

ARTICLE OPEN



Multiplexed neurochemical transmission emulated using a dual-excitatory synaptic transistor

Mingxue Ma¹, Yao Ni¹, Zirong Chi¹, Wanqing Meng², Haiyang Yu¹, Jiangdong Gong¹, Huanhuan Wei¹, Hong Han¹, Xinran Wang² and Wentao Xu¹  

The ability to emulate multiplexed neurochemical transmission is an important step toward mimicking complex brain activities. Glutamate and dopamine are neurotransmitters that regulate thinking and impulse signals independently or synergistically. However, emulation of such simultaneous neurotransmission is still challenging. Here we report design and fabrication of synaptic transistor that emulates multiplexed neurochemical transmission of glutamate and dopamine. The device can perform glutamate-induced long-term potentiation, dopamine-induced short-term potentiation, or co-release-induced depression under particular stimulus patterns. More importantly, a balanced ternary system that uses our ambipolar synaptic device backtrack input 'true', 'false' and 'unknown' logic signals; this process is more similar to the information processing in human brains than a traditional binary neural network. This work provides new insight for neuromorphic systems to establish new principles to reproduce the complexity of a mammalian central nervous system from simple basic units.

npj 2D Materials and Applications (2021)5:23; <https://doi.org/10.1038/s41699-021-00205-4>

INTRODUCTION

Brain-inspired neuromorphic computing on the hardware level can achieve high efficiency in performing cognitive and data-intensive tasks^{1,2}. However, most reports on artificial synapses (ASs) have focused only on improving single-neurotransmitter induced synaptic plasticity, instead of exploiting complex synaptic activities that are also significant in a human brain^{3–9}. Multiplexed neurotransmission is a mixture of independent-release and co-release of different neurotransmitters from distinct microdomains of the same axon; this mechanism underlies diverse functions of the ventral tegmental area (VTA) region in the midbrain¹⁰. The ability of our brain to select an appropriate function and subsequent respond to a complex external environment requires multiplexed neurotransmission^{11–13}. However, fabrication of an AS that can emulate multiplexed neurotransmission has been a challenging task, owing to constraints imposed by the unipolar characteristics, or unreliability of bipolar characteristics in individual devices.

Furthermore, the previous reported ASs can only distinguish 'true' from 'false', by applying stimulus to realize Boolean logic^{14–16}. However, information processing in a human brain operates more like a balanced ternary system for judging 'true', 'false', and 'unknown', rather than a binary system¹⁷. That ability requires a balanced ternary system that is compatible with multiplexed neurotransmission, providing the possibility of fuzzy computing and autonomous learning under a complex external environment.

In this work, we exploit the tunability of charge-carrier polarity in two-dimensional (2D) layered-PdSe₂ material to mimic multiplexed neurotransmission in a midbrain biological synapse that can co-release two neurotransmitters: dopamine and glutamate. These are two principal excitatory neurotransmitters that are involved in multiplexed neurotransmission to co-trigger the stimulation of the autonomic nervous system, and create thinking

and impulse signals^{18–21}. This ability is attributed to the use of ambipolar PdSe₂, which is selected because its interplanar spacing is larger than TFSI (bis(trifluoromethylsulfonyl)imide) anions but much smaller than EMIM (1-ethyl-3-methylimidazolium) cations in ion-gel dielectric layer²². Besides the independent excitatory effect of glutamate or dopamine, the device also achieved inhibitory effects of co-release of the two neurotransmitters. By exploiting this unique three-working-regime feature, our PdSe₂ synapse realizes logic operation similar to that of a balanced ternary system to backtrack input logic signals. 2D layered PdSe₂ was chosen because the majority of charge carriers can be switched between holes and electrons^{23,24}. This synaptic device is distinct from the previous excitatory and inhibitory ASs in both functional mechanism and biological plasticity^{25–27}. This work demonstrates that PdSe₂ and other ambipolar 2D materials are candidate materials for using in future neuroelectronic devices that have brain-inspired complexity.

RESULTS

Device structure and material characteristics

Some subgroups of VTA neurons (Fig. 1, top) can release dopamine and glutamate from the same axonal terminals. The two excitatory neurotransmitters can interact with receptors on the postsynaptic membrane either independently or synergistically. A proposed synaptic device structure (Fig. 1, bottom) to emulate these behaviors uses layered PdSe₂ semiconductor as the active channel. The on-top ion-gel layer simulates the end of a presynaptic neuron that can release two types of excitatory neurotransmitters depending on presynaptic spikes. We used the TFSI anions and EMIM cation in the ion-gel to mimic the function of glutamate and dopamine, respectively. The PdSe₂ conductive channel that connects source and drain electrodes functions as

¹Institute of Photoelectronic Thin Film Devices and Technology, Key Laboratory of Optoelectronic Thin Film Devices and Technology of Tianjin, Engineering Research Center of Thin Film Optoelectronics Technology of Ministry of Education, College of Electronic Information and Optical Engineering, National Institute for Advanced Materials, Nankai University, Tianjin 300350, P.R. China. ²National Laboratory of Solid State Microstructures, School of Electronic Science and Engineering and Collaborative Innovation Center of Advanced Microstructures, Nanjing University, Nanjing 210023, P.R. China. ✉email: wentao@nankai.edu.cn

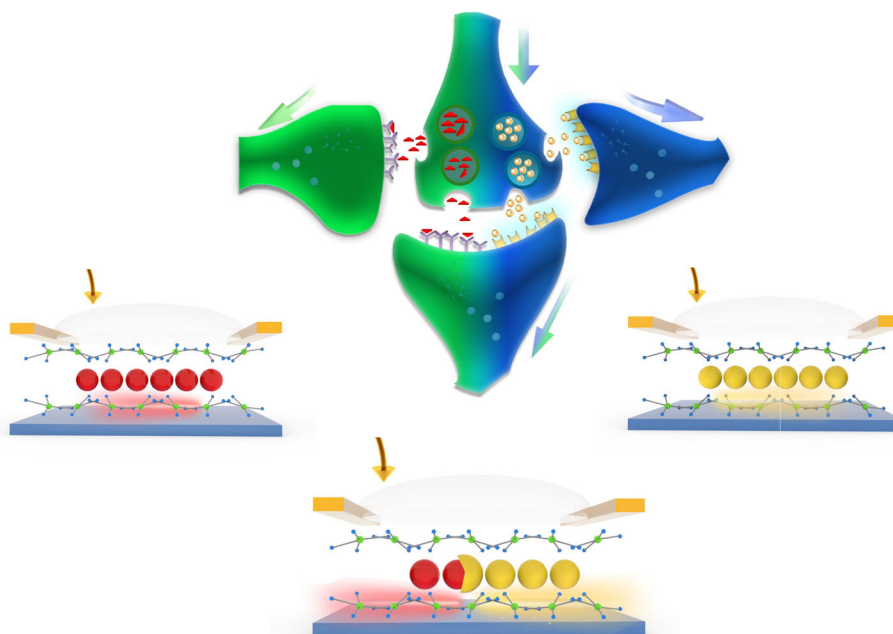


Fig. 1 Dual-excitatory PdSe₂ artificial synapse. Schematic of biological synapse that can release two types of excitatory neurotransmitters, glutamate (red triangle), and dopamine (yellow circle), from a single presynaptic membrane; these neurotransmitters can interact with receptors on the postsynaptic membrane either independently or synergistically (top). Schematic of artificial synaptic device based on layered PdSe₂ (bottom). When the device received negative presynaptic spikes, the hole (red sphere) accumulate in the conduction channel and the increasing hole currents simulate the postsynaptic glutamate currents (bottom left); when device received positive presynaptic spikes after negative spikes, the electrons (yellow sphere) began to neutralize holes, and the decreasing hole currents simulate the decreasing postsynaptic glutamate currents induced by inhibitory effect between glutamate and dopamine interaction (bottom middle); when the device continued to receive positive presynaptic spikes, the electrons accumulated in the conduction channel and the increasing electron currents simulated the postsynaptic dopamine currents (bottom right).

the postsynaptic membrane, in which the two excitatory neurotransmitters work independently to induce long-term or short-term excitatory effects (Fig. 1, bottom left and bottom right devices), and synergistically to cause a reciprocal inhibitory effect (Fig. 1, bottom middle device). The postsynaptic response can be regulated over a wide range of characteristics by just tuning the polarity of the pulse that is applied to the input terminal, or the bias condition between the drain electrode and source electrode.

A high-resolution transmission electron microscope (HRTEM) image (Fig. 2a) shows the lattice fringes of the PdSe₂ film, and reveals that the interplanar spacing is ~ 0.3 nm with orientation along (002) direction, as reported previously²³. Comparing the size of the cations and anions in the ion gel (Fig. 2b) with the interplanar spacing ~ 0.3 nm along (002) direction of PdSe₂ film, the anions can be injected into the PdSe₂ film, whereas the cations cannot be injected, because they are much larger than the anions. Energy-dispersive X-ray spectroscopy (EDXS) determined that the atomic ratio Pd:Se was close to 1:2 (Fig. 2c and Supplementary Fig. 1a). A selective area electron diffraction (SAED) pattern (Fig. 2d) confirmed that the PdSe₂ film is polycrystalline. Atomic force microscope (AFM) (Fig. 2e) revealed that the PdSe₂ film is about 5.04-nm thick, and is therefore effectively a 2D structure. The X-ray diffraction (XRD) pattern (Supplementary Fig. 1b) shows peaks at 22.8° and 41.6°, which shows a strong gain orientation along the *c* axis owing to the layered crystal structure along the *c* axis and well agrees with the crystal structure of PdSe₂ revealed by HRTEM image of the (002) planes²³. The Raman spectrum (Fig. 2f) shows four main distinct peaks (at ≈ 143 , ≈ 206 , ≈ 223 , and ≈ 256 cm⁻¹); the three peaks at low wavenumber related to the movement modes of Se atoms, and the strongest mode is correspond to the relative movement between Pd and Se atoms²⁴.

Functional mechanism of dual-excitatory artificial synapse

Transfer curves (Fig. 3a) at different drain voltages V_d were measured under dual-sweeping gate voltage V_g from 4 to -4 V. The hysteresis loops in the hole-transport-dominated conduction (HTDC) region is obviously larger than those in the electron-transport-dominated conduction (ETDC) region. X-ray photoelectron spectroscopies (XPS) was performed to further confirm TFSI anions is more likely than EMIM cations to be injected into layered PdSe₂. The PdSe₂ films were covered by ion-gel and treated by a train of $+6$ V ($N=300$) and -6 V ($N=300$) gate voltage, respectively. The XPS core-levels of the main Pd 3d (Supplementary Fig. 1c) and Se 3d (Supplementary Fig. 1d) for PdSe₂ film were collected before and after voltage treatment. For pristine PdSe₂, the binding energies of Pd 3d_{3/2} is 342.2 eV and binding energies of Se 3d_{3/2} is 55.8 eV. After -6 V ($N=300$) treatment, the core-level peaks of Pd 3d_{3/2} (342.3 eV) and Se 3d_{3/2} (55.9 eV) in PdSe₂ show a uniform shift toward higher binding energies compared to those of the pristine PdSe₂. This upshift of peaks is attributed to the valence band maximum shifts away from the Fermi energy due to the doping of the TFSI anions²⁸. However, after $+6$ V ($N=300$) treatment, the core-level peaks of Pd 3d_{3/2} (342.2 eV) and Se 3d_{3/2} (55.8 eV) in PdSe₂ show no shift. This indicates that the EMIM cations cannot be charged into PdSe₂ film. Therefore, an intermediate transition (IT) region will occur when presynaptic spikes are changed from negative to positive. This characteristic means that the entire working window of our device can be divided naturally into three regions: HTDC, IT, and ETDC.

The contour map (Fig. 3b) of drain current I_d is displayed to visualize the three regions, the color in the $I-V$ contour map represents the amplitude of $\log(I_d)$. We can emulate the glutamate-independent excitatory-effect in the HTDC region (Fig. 3a, pink region and Fig. 3b, region one), the glutamate-and-dopamine synergistic inhibitory-effect in the IT region (Fig. 3a, green region

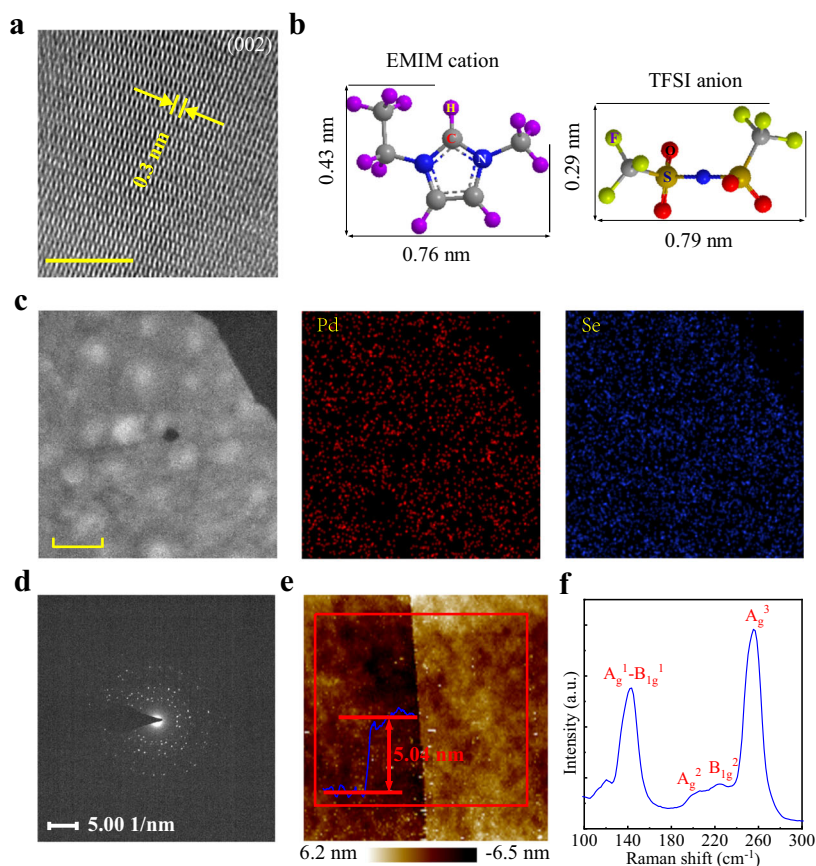


Fig. 2 **Material characteristics.** **a** STEM image of the lattice fringes of the 2D PdSe₂ reveals that the interplanar spacing along (002) direction is ~0.3 nm, scale bar: 5 nm. **b** Chemical structures and size dimension of EMIM cation and TFSI anion in the ion-gel. **c** EDXS element mapping of 2D PdSe₂ reveals that the atomic ratio Pd:Se is close to 1:2, scale bar: 50 nm. **d** SAED pattern of the polycrystalline lattice structure of 2D PdSe₂ film. **e** AFM image with height profile of the 2D PdSe₂. **f** Room-temperature Raman spectra of the 2D PdSe₂.

and Fig. 3b, region two), and the dopamine-independent excitatory-effect in the ETDC region (Fig. 3a, organ region and Fig. 3b, region three).

The releasing of glutamate from presynaptic membrane can be mimicked in the HTDC region (Fig. 3c top panel). When a negative presynaptic spike was applied to a W-probe that contacted the ion gel, the cations in the gel surrounded the probe, and anions accumulated at the ion-gel/PdSe₂ interface or were even injected into PdSe₂ film and thereby increasing the channel conductivity for a relatively long time (Fig. 3c, bottom panel). This behavior offers our PdSe₂ synapse the ability to form relative long-term memory in the HTDC region.

In the IT region, we mimicked the releasing of both glutamate and dopamine from a single presynaptic membrane (Fig. 3d, top panel). When positive spikes were applied to the device after negative spikes, the electron combined with hole and thereby neutralized them, so hole current decreased; the injected anions were not removed from PdSe₂ film completely, so hole current was not eradicated because holes still dominate the conduction through the synapse (Fig. 3d, bottom panel). As a result, the process of changing the presynaptic spike from negative to a small positive voltage does not immediately convert the p-type conduction state to the n-type conduction. The hole-current decrease that is induced by electrons neutralizing holes resembles the behavior in which dopamine activates D2-family receptors and thereby decreases postsynaptic glutamate currents in rodents and in the human brain cortex.

The releasing of dopamine from the presynaptic membrane can be emulated in the ETDC region (Fig. 3e, top panel). When the

device receives a large enough positive voltage or a huge number of positive spikes, the electrons eventually dominate the conduction state. With a positive presynaptic spike, the cations accumulated at the ion-gel/PdSe₂ interface, and thereby induced electron generation in the PdSe₂ channel (Fig. 3e, bottom panel).

The entire transform procession of our device can be summarized schematically. In HTDC region, the corresponding EPSCs (Fig. 3f) that are triggered by a negative spike (−3 V, 50 ms) and opposite drain voltages stimulate a relatively long (>10 s) increase in magnitude of current. In the IT region, the corresponding inhibitory postsynaptic currents (IPSCs) can be obtained (Fig. 3g) by applying a relatively small positive spike (1 V, 50 ms). In the ETDC region, the corresponding EPSCs triggered by a relatively large positive spike (3.5 V, 50 ms) (Fig. 3h) and opposite drain voltages maintain the current for a relatively short time (<2 s).

The change of presynaptic spike from positive to small negative voltage occurred with almost no intermediate transition state (Supplementary Fig. 2), because many electron traps occurred between PdSe₂ film and P⁺⁺/Si/SiO₂ substrate, so free positive charges dominated the device in the absence of V_g, and the cations were difficult to inject into the PdSe₂ film^{29,30}. Therefore long-term memory is not likely to form in the ETDC region.

Electrical behaviors of three synaptic plasticity modes

We firstly emulate the independent excitatory effect of glutamate in the HTDC region. Glutamate is a principal excitatory neurotransmitter that works at a variety of excitatory synapses in the

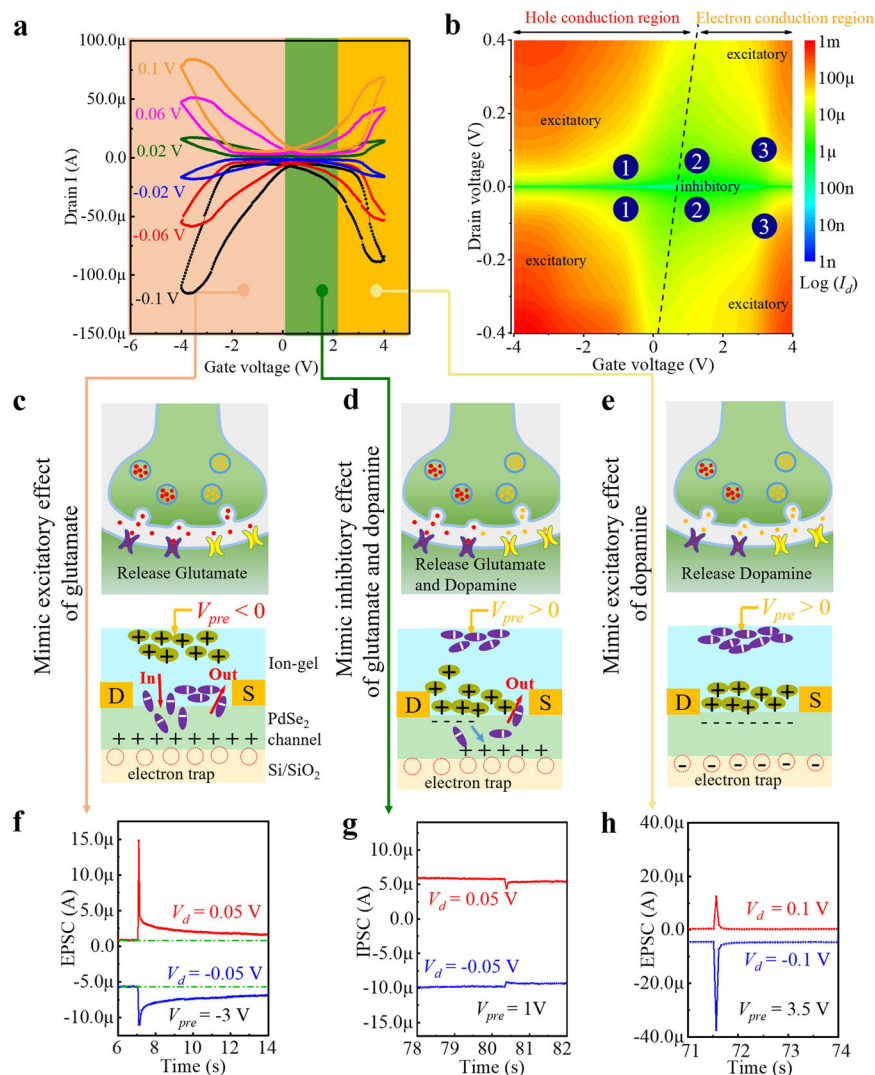


Fig. 3 A better understanding of dual-excitatory operation mechanism. **a** Dual-sweep $I_d - V_g$ transfer curves of the device under $V_d = \pm 0.02, \pm 0.06, \pm 0.1$ V. The entire working window can be divided into three regions corresponding to a glutamate-independent excitatory effect region, a glutamate-and-dopamine synergistic inhibitory effect region, and a dopamine-independent excitatory effect region, respectively. **b** The current measured at the drain electrode was plotted as a function of V_d and V_g ; the color in the $I - V$ contour map represents the amplitude of $\log(I_d)$ and the three regions are clearly distinguished by the color. **c** Anions in the ion gel simulated the glutamate. Application of a negative presynaptic spike V_{pre} induce holes accumulation in the conduction channel, and hole current represents glutamatergic postsynaptic current. **d** Hole-current decrease induced by electrons progressively neutralizing holes represents the inhibitory effect between glutamate and dopamine. **e** Cations in the ion gel simulate dopamine. Continuing application positive presynaptic spikes induces electrons accumulation in the conduction channel; electron-current represents dopaminergic postsynaptic current. **f** EPSCs in response to a -3 V input pulse were read with the polarity opposite reading voltages. **g** IPSCs in response to a relatively small positive 1 V input pulses were read with the polarity opposite reading voltage. **h** The EPSCs in response to a large enough positive 3.5 V input pulse were read with the polarity opposite reading voltage.

mammalian brain, and is involved in learning and formation of memory¹⁸. The change of synaptic weight in a brain is regarded as the basis of the learning and memory. The synaptic weight can be tuned by adjusting the amplitude, duration, frequency, and number of stimuli. The formation of memory requires a change of synaptic weight that lasts a long time (minutes to hours, even years)³¹. Our device showed paired-pulse facilitation (PPF), evoked by a pair of identical pre-synaptic spikes (Fig. 4a). The second EPSC (A2) had 26.6% higher amplitude than the first EPSC (A1). When the first spike was applied on the gate electrode, anions in gel moved to the interface and injected into the PdSe₂ film. However, the second input spike arrived before all of the anions could return to their equilibrium sites, so the second EPSC was larger than the first one. The PPF index correlates with the time interval (Δt) between pre-synaptic spikes; PPF slowly decayed as Δt

increased (Fig. 4b). The experimental data was fitted by an exponential function. When two trains of presynaptic spikes (-3 V, 50 ms) with different frequency f were applied to the devices, the postsynaptic currents increased significantly with the increase of frequency (Fig. 4c). The currents after 85 s were ~ 4.4 ($f = 0.5$ Hz) and 8.6 μ A ($f = 10$ Hz), which are 47 and 177% larger than the resting current of 3.0 μ A. Two other $0.5 \leq f \leq 10$ Hz were also applied on our device (Supplementary Fig. 3a).

When the spike amplitude was increased, the EPSCs also increased, so the duration for which the postsynaptic current increased was extended (Fig. 4d). The postsynaptic currents also increased with increase in the number of spikes (Fig. 4e). After 20 s, the current I_t at time t s increased over resting current I_0 by change ratios $((I_t - I_0)/I_0 \times 100\%)$ 80% (one spike), 350% (30 spikes), and 550% (100 spikes). After 10^3 s, the current triggered by

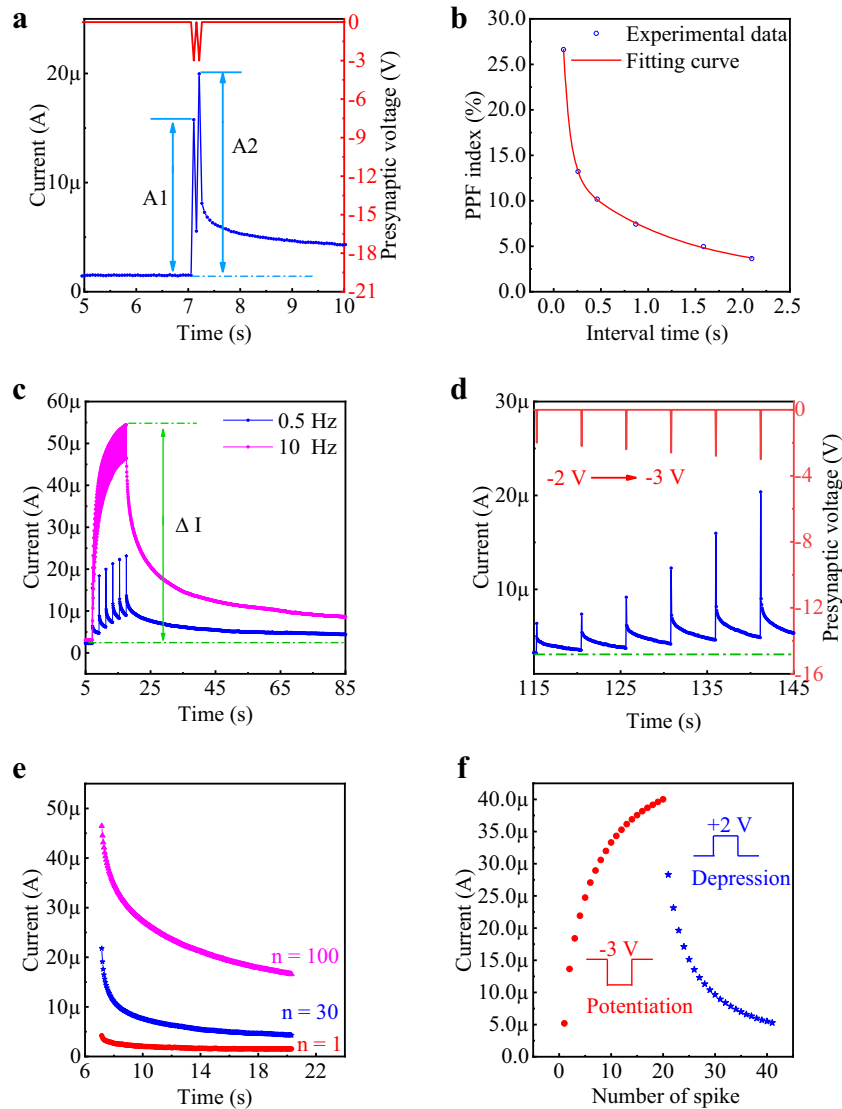


Fig. 4 Long-term plasticity. **a** EPSCs triggered by two identical spikes, with an interval of 104 ms. Amplitudes of the first and second EPSCs are A1 and A2, respectively. **b** PPF index versus time interval between two successive input pulses. **c** Current change at different frequency of pulse stimulations. **d** EPSCs triggered by a series of different presynaptic spikes from -2 to -3 V in step of -0.2 V. **e** Postsynaptic current versus time stimulated by different number of presynaptic spikes. **f** Potentiation and depression triggered by 19 negative and 21 positive pulses.

100 spikes was still higher than I_0 (Supplementary Fig. 3b). Therefore, the transition from short-term memory to long-term memory was realized in our device.

In addition, Potentiation and depression as important forms of long-term plasticity were demonstrated in our device by consecutively applying 19 negative (-3 V, 50 ms) and 21 positive (2 V, 50 ms) spikes at the presynaptic input terminal, the postsynaptic current increased with the negative input spikes, and then decreased with the positive input spikes (Fig. 4f).

Then we quantified synergetic inhibitory effect of glutamate and dopamine interaction in the IT region, and the independent excitatory effect of dopamine in the ETDC region. In biology, glutamate shows excitotoxicity, in which an excessive release of glutamate neurotransmitters can cause the death of neurons³². Biological synapses can avoid this overreaction by using dopamine to inhibit the synaptic excitation that glutamate induces³³. We have proved that both positive and negative spikes can induce an excitatory response in our PdSe₂ synapse, but if a positive spike is applied too soon after a negative spike or before

the disappearance of its effect, the positive spike induces an inhibitory response. The postsynaptic current underwent potentiation, depression, and re-potentiation when our synapse received 30 negative pulses then 60 positive pulses (Fig. 5a, b).

This transformation can also be achieved by changing the amplitude or duration of the spikes. When a train of positive spikes with increasing amplitude was applied to the device, an obvious transition from IPSC to EPSC occurred (Fig. 5c). The reason is that electrons continuously neutralize holes until electrons dominate the conduction. This phenomenon is similar to the inhibitory effect between glutamate and dopamine. When a spike duration was increased, EPSC initially changed to IPSC, but then re-changed to EPSC as the duration increased (Fig. 5d).

To see the inhibitory effect directly, we conducted a spatio-temporal experiment, in which two spikes were applied simultaneously to the corresponding gates (Fig. 5e). When presynaptic input terminal 1 (P1) and presynaptic input terminal 2 (P2) were both single negative spike (-3 V, 214 ms), the triggered EPSC = 39.8 μ A (Fig. 5f, first peak). This current remained above the initial

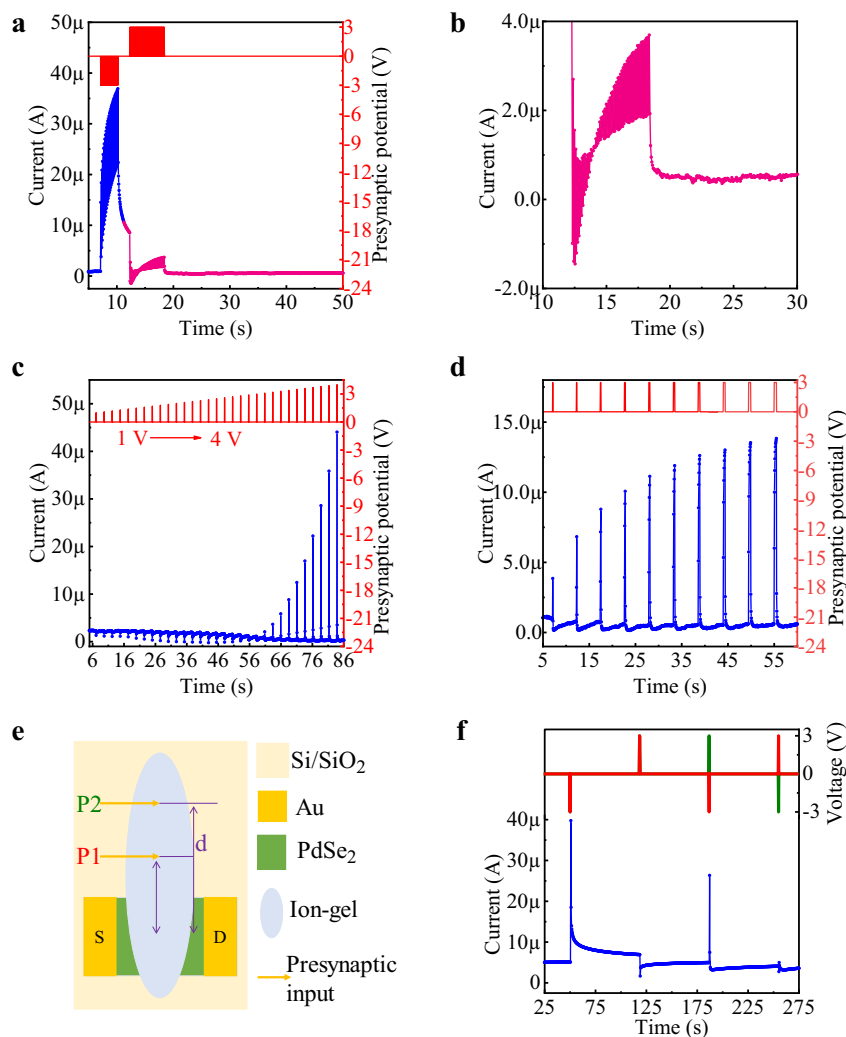


Fig. 5 Neurotransmitters interaction and short term plasticity. **a** Postsynaptic currents stimulated by 30 negative and 60 positive pulses. **b** Magnified image of postsynaptic current in the dotted rectangle in **(a)**. **c** Postsynaptic currents triggered by different amplitudes (from 1 to 4 V, with a step of 0.1 V) of presynaptic spike. **d** Postsynaptic currents triggered by different durations (from 51 to 510 ms, with a step of 51 ms) of presynaptic spike. **e** Schematic of AS with two input terminals; the perpendicular distance between the input terminal and the center of the channel is **(d)**. **f** Integrated postsynaptic currents recorded in response to two spatially-correlated input terminals with different combinations of input voltages.

current until both P1 and P2 were treated simultaneously with a single positive spike (3 V, 481 ms). The electrons depleted the holes, so the positive spikes triggered IPSC = 1.7 μ A (Fig. 5f, second peak).

When a single negative spike (−3 V, 214 ms) was applied to P1 simultaneously with a single positive spike (3 V, 214 ms) applied to P2, the postsynaptic current first increased, then decreased, then increased again (Fig. 5f, third peak). The current after the spikes is lower than the current before the spikes, so this is an inhibitory response. This pattern occurs because P1 is closer than P2 to the center of the channel, so the anions arrived at the postsynaptic membrane before the cations.

When a single positive spike (3 V, 214 ms) was applied to P1 simultaneously with a single negative spike (−3 V, 214 ms) to P2, the postsynaptic current first decreased, then increased, then decreased (Fig. 5f, fourth peak). The current after the spikes was lower than the current before the spikes, this is also an inhibitory response.

These results confirmed that our synaptic device can simulate the synergetic inhibitory effect between neurotransmitters, in which inhibitory behavior is elicited when one kind of excitatory

neurotransmitter arrives at the postsynaptic membrane before the effect of another kind of excitatory neurotransmitter disappears.

In all the above cases, when the EPSC was induced by the accumulation of electrons, the current showed almost no change after the spike applied. To further confirm this, we firstly changed the conduction dominated by the electron, then applied five trains of spikes (3 V, 50 ms) with different f to the devices. The postsynaptic currents increased significantly with increase in f (Supplementary Fig. 4), but the change lasted a very short time (<2 s). This result indicated that in the ETDC region, our artificial device can extract and transfer information rapidly and efficiently when receiving a huge number of stimuli.

We also confirmed that the same independent excitatory effect of glutamate, synergetic inhibitory effect of glutamate and dopamine interaction, and independent excitatory effect of dopamine can be achieved by our PdSe₂ synapse when negative driving voltage are applied. In HTDC region, the corresponding spike-rate dependent plasticity (Supplementary Fig. 5a) and spike-number dependent plasticity (Supplementary Fig. 5b) identical show the long-term memory. In IT region and ETDC region, the corresponding potentiation, depression, and re-potentiation

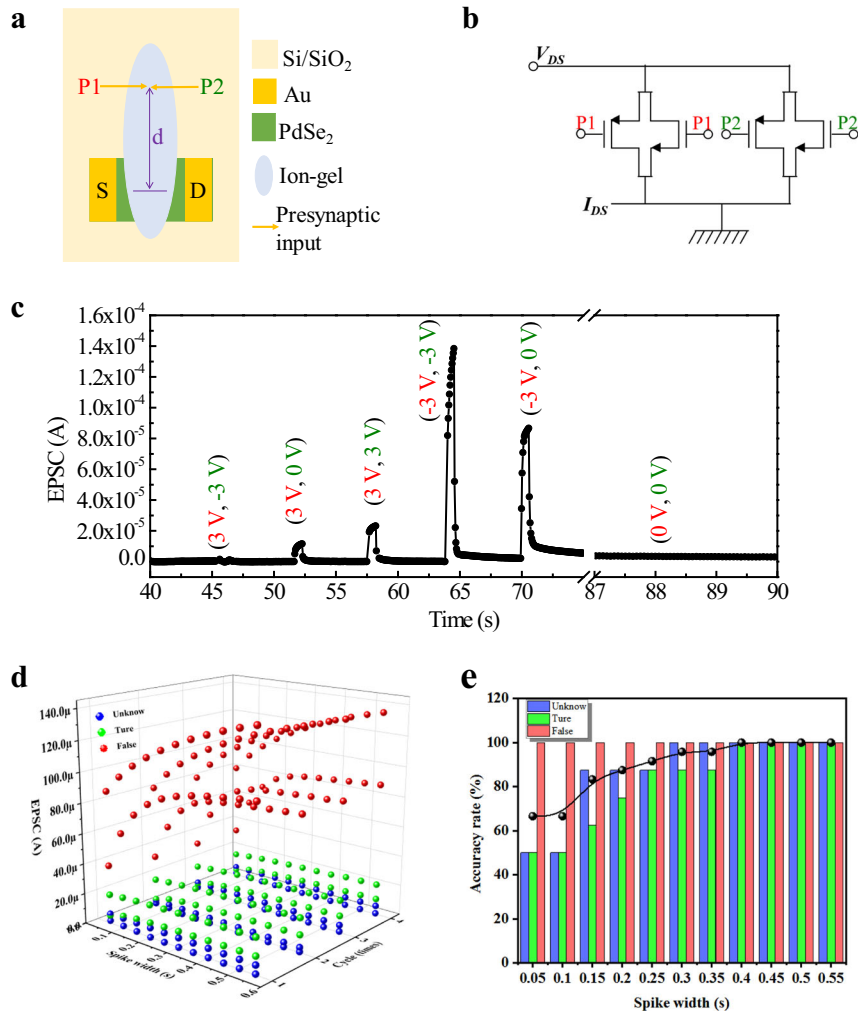


Fig. 6 Input logic signals backtrack. **a** Schematic image of AS with two input terminals that have identical distances from the center of the channel. **b** The normal logic circuits that can integrate memory and computation. **c** Different magnitudes of postsynaptic current stimulated by six different combinations of input logic signals. **d** Data set were collected to train SVM. **e** The result of analogous simulation, which shows with the increasing of the spike duration the accuracy can achieve 100%.

(Supplementary Fig. 5c) and spike-voltage dependent plasticity (Supplementary Fig. 5d) also exhibit the same behavior as positive driving voltage. Therefore, the postsynaptic response can be regulated over a wide range of characteristics by just tuning the polarity of the pulse that is applied to the input terminal, or the bias condition between the drain electrode and source electrode.

Input logic signals backtrack

The unique dual-excitatory of PdSe₂ synapse allows the dual-gate AS to simulate the similar logic operation of balanced ternary to backtrack input logic signals. By applying two spikes simultaneously at the same place on the ion gel, this AS was treated as a memory and computation-integrated balanced ternary memory cell of a static random access memory system (Fig. 6a). In normal logic circuits, the same function requires at least four transistors (Fig. 6b). The logic signal -1, 0, and 1 in the balanced ternary represent 'false', 'unknown', or 'true', respectively; and three voltage spike signals -3, 0, and 3 V applied on our device correspond to logic signal -1, 0, and 1, respectively. Taking advantage of the dual-excitatory and significant current value difference induced by positive and negative spikes, the postsynaptic current values at different logic signal combinations were distinguished (Fig. 6c).

Different output currents that contain input signal information were induced by the combinations of input signals: 'P1 = -1' and ('P2 = -1' or 'P2 = 0') yielded logic -1 (=false). 'P1 = -1' and ('P2 = 1' or 'P1 = 0' and 'P2 = 0') yielded logic 0 (=unknown). 'P1 = 1' and ('P2 = 1' or 'P2 = 0') yielded logic 1 (=true). The relatively independent current range for each output value provides the possibility to backtrack input signals.

To study the accuracy of this backtrack, the above mentioned six input-signal combinations with spike durations from 0.05 to 0.55 s were applied to the device. We repeated the measurement for four cycles as a training data set (Fig. 6d), then we input the training data set into Support Vector Machine to give it the ability to implement classification. After this training process, we measured four additional cycles of test data to input into the Support Vector Machine model for simulation (Supplementary Fig. 6a). As spike duration was increased, the accuracy of backtracking increased to 100% (Fig. 6e and Supplementary Fig. 6b). Equation and parameters (Supplementary Fig. 7) used in Support Vector Machine. Therefore, the dual-excitatory feature of our PdSe₂ synapse emulated the similar logic operation of balanced ternary logic to backtrack the input logic signals successfully. Compared to the binary system, ternary logic is closer to the thinking method in a human brain and can provide the capability for fuzzy computing and autonomous learning in future computers.

DISCUSSION

In summary, a dual-excitatory AS based on few-layer PdSe₂ is fabricated to emulate the independent and synergetic effect of two types of excitatory neurotransmitters that are released from the same neuron. The entire working window of our PdSe₂ synapse can be naturally divided into three distinct regions: HTDC region, IT region, and ETDC region. Glutamate-induced long-term excitatory effect, dopamine-induced short-term excitatory effect, and reciprocal inhibitory effect of the two neurotransmitters could be emulated in these regions, respectively. More importantly, logic operation of a balanced ternary system has been achieved in our dual-excitatory AS, which provides a practical way for the next generation of artificial intelligence. This work provides a new way to enrich the function of the AS and its application to neuromorphic computing.

METHODS

Fabrication of the devices

Few-layer PdSe₂ film grown on P⁺⁺Si/300 nm SiO₂ by chemical vapor deposition was purchased from Sixcarbon Technology. The source and drain Au electrodes (60 nm) were thermally deposited through an interdigital shadow mask (width 1500 μm; length 40 μm) onto the PdSe₂ films. Then the ion-gel top-gate dielectric (the mass ratio between polymer Poly(vinylidene fluoride-co-hexafluoropropylene) PVDF-HFP and ionic liquid 1-ethyl-3-methylimidazolium bis(trifluoromethylsulfonyl)imide EMIM-TFSI is 1:3) layer was transferred onto the channel area. A metal probe that contacted the ion gel was used to apply the presynaptic spike, which is the presynaptic input terminal.

Characterizations

XRD patterns were obtained using a Rigaku Ultima IV instrument. A Bruker Dimension Icon microscope in tapping mode was used to obtain the AFM images. HRTEM images obtained using a FEI Talos F200X microscope. The element mapping (Fig. 1c and Fig. S1a) was acquired using a build-in EDXS measurement module in the TEM system. The Raman spectrum were obtained using a TEO SR-5001-A system under 532-nm excitation line. XPS measurement was performed using Thermo Scientific Escalab 250Xi. All electrical measurements were performed using a Keithley 4200A semiconductor parameter analyzer and a probe station in N₂ environment in a glove box at room temperature.

DATA AVAILABILITY

The datasets generated during and/or analyzed during the current study are available from the corresponding author on reasonable request. All data generated or analyzed during this study are included in this published article (and its Supplementary Information).

Received: 19 August 2020; Accepted: 4 December 2020;

Published online: 22 February 2021

REFERENCES

- van de Burgt, Y., Melianas, A., Keene, S. T., Malliaras, G. & Salleo, A. Organic electronics for neuromorphic computing. *Nat. Electron.* **1**, 386–397 (2018).
- Wan, Q., Sharbati, M. T., Erickson, J. R., Du, Y. & Xiong, F. Emerging artificial synaptic devices for neuromorphic computing. *Adv. Mater. Technol.* **4**, 1900037 (2019).
- Ohno, T. et al. Short-term plasticity and long-term potentiation mimicked in single inorganic synapses. *Nat. Mater.* **10**, 591–595 (2011).
- Gkoupidenis, P., Schaefer, N., Garlan, B. & Malliaras, G. G. Neuromorphic functions in PEDOT:PSS organic electrochemical transistors. *Adv. Mater.* **27**, 7176–7180 (2015).
- Xu, W. et al. Organometal halide perovskite artificial synapses. *Adv. Mater.* **28**, 5916–5922 (2016).
- Park, Y. & Lee, J. S. Artificial synapses with short- and long-term memory for spiking neural networks based on renewable materials. *ACS Nano* **11**, 8962–8969 (2017).
- van de Burgt, Y. et al. A non-volatile organic electrochemical device as a low-voltage artificial synapse for neuromorphic computing. *Nat. Mater.* **16**, 414–418 (2017).

- Xu, W. T. et al. Ultrasensitive artificial synapse based on conjugated polyelectrolyte. *Nano Energy* **48**, 575–581 (2018).
- Kim, K., Chen, C. L., Truong, Q., Shen, A. M. & Chen, Y. A carbon nanotube synapse with dynamic logic and learning. *Adv. Mater.* **25**, 1693–1698 (2013).
- Barker, D. J., Root, D. H., Zhang, S. & Morales, M. Multiplexed neurochemical signaling by neurons of the ventral tegmental area. *J. Chem. Neuroanat.* **73**, 33–42 (2016).
- Munster-Wandowski, A., Gomez-Lira, G. & Gutierrez, R. Mixed neurotransmission in the hippocampal mossy fibers. *Front. Cell. Neurosci.* **7**, 210 (2013).
- Yu, X. et al. Wakefulness is governed by GABA and histamine cotransmission. *Neuron* **87**, 164–178 (2015).
- Andre, V. M., Cepeda, C. & Levine, M. S. Dopamine and glutamate in Huntington's disease: a balancing act. *CNS Neurosci. Ther.* **16**, 163–178 (2010).
- Liu, Y. Q. et al. Self-powered artificial synapses actuated by triboelectric nanogenerator. *Nano Energy* **60**, 377–384 (2019).
- Wan, C. J. et al. Flexible metal oxide/graphene oxide hybrid neuromorphic transistors on flexible conducting graphene substrates. *Adv. Mater.* **28**, 5878–5885 (2016).
- Zhu, L. Q. et al. Flexible proton-gated oxide synaptic transistors on Si membrane. *ACS Appl. Mater. Interfaces* **8**, 21770–21775 (2016).
- Jeong, J. W. et al. Tunneling-based ternary metal–oxide–semiconductor technology. *Nat. Electron.* **2**, 307–312 (2019).
- McEntee, W. J. & Crook, T. H. Glutamate: its role in learning, memory, and the aging brain. *Psychopharmacology* **111**, 391–401 (1993).
- Bromberg-Martin, E. S., Matsumoto, M. & Hikosaka, O. Dopamine in motivational control: rewarding, aversive, and alerting. *Neuron* **68**, 815–834 (2010).
- David, S. et al. Dopamine neurons make glutamatergic synapses in vitro. *J. Neurosci.* **18**, 4588–4602 (1998).
- Tseng, K. Y. & O'Donnell, P. Dopamine–glutamate interactions controlling prefrontal cortical pyramidal cell excitability involve multiple signaling mechanisms. *J. Neurosci.* **24**, 5131–5139 (2004).
- Huang, H. C., Huang, C. W., Hsieh, C. T. & Teng, H. Electric double layer capacitors of high volumetric energy based on ionic liquids and hierarchical-pore carbon. *J. Mater. Chem. A* **2**, 14963–14972 (2014).
- Chow, W. L. et al. High mobility 2D palladium diselenide field-effect transistors with tunable ambipolar characteristics. *Adv. Mater.* **29**, 1602969 (2017).
- Zeng, L. H. et al. Controlled synthesis of 2D palladium diselenide for sensitive photodetector applications. *Adv. Funct. Mater.* **29**, 1806878 (2019).
- Tian, H. et al. Graphene dynamic synapse with modulatable plasticity. *Nano. Lett.* **15**, 8013–8019 (2015).
- Tian, H. et al. Emulating bilingual synaptic response using a junction-based artificial synaptic device. *ACS Nano* **11**, 7156–7163 (2017).
- Tian, H. et al. Anisotropic black phosphorus synaptic device for neuromorphic applications. *Adv. Mater.* **28**, 4991–4997 (2016).
- Zhang, S. et al. Controllable, wide-ranging n-doping and p-doping of monolayer group 6 transition-metal disulfides and diselenides. *Adv. Mater.* **36**, 1802991 (2018).
- Ni, Y. et al. Effective performance improvement of organic thin film transistors by using tri-layer insulators. *Eur. Phys. J. -Appl. Phys.* **83**, 20201 (2018).
- Pei, K. et al. A high-performance optical memory array based on inhomogeneity of organic semiconductors. *Adv. Mater.* **30**, e1706647 (2018).
- Ren, Y. et al. Ambipolar transistors: recent advances in ambipolar transistors for functional applications. *Adv. Funct. Mater.* **29**, 1903700 (2019).
- Nishizawa, Y. Glutamate release and neuronal damage in ischemia. *Life Sci.* **69**, 369–381 (2001).
- Rubinstein, M. et al. Dopamine D4 receptor-deficient mice display cortical hyperexcitability. *J. Neurosci.* **21**, 3756–3763 (2001).

ACKNOWLEDGEMENTS

This research is supported by Guangdong Key R&D Project (2018B030338001), the Fundamental Research Funds for the Central Universities (075-63191740, 075-63191745, 075-92022027), Tianjin Science Foundation for Distinguished Young Scholars (Grant No. 19JCJC61000), Hundred Young Academic Leaders Program of Nankai University (2122018218), Natural Science Foundation of Tianjin (18JCYBJC16000), the National Natural Science Foundation of China (NSFC, 51573036), the 111 Project (B16027), the International Cooperation Base (2016D01025), Tianjin International Joint Research and Development Center, Graduate research and innovation project of Tianjin (2019YJSS089).

AUTHOR CONTRIBUTIONS

W.X. initiated the research. W.X., M.X.M., and Y.N. designed the experiments. M.X.M. and Y.N. collected the data. M.X.M. and W.X. analyzed the data and designed the

manuscript. Y.N. and Z.R.C. contributed to the analog simulation. W.Q.M and H.Y.Y. analyzed and discussed the data. W.Q.M, J.D.G., H.H.W., and H.H. contributed to the design of the figures. W.X. and X.W. supervised the research. All authors discussed the results and commented on the manuscript. M.X.M. and Y.N. contributed equally to this work.

COMPETING INTERESTS

The authors declare no competing interests.

ADDITIONAL INFORMATION

Supplementary information The online version contains supplementary material available at <https://doi.org/10.1038/s41699-021-00205-4>.

Correspondence and requests for materials should be addressed to W.X.

Reprints and permission information is available at <http://www.nature.com/reprints>

Publisher's note Springer Nature remains neutral with regard to jurisdictional claims in published maps and institutional affiliations.



Open Access This article is licensed under a Creative Commons Attribution 4.0 International License, which permits use, sharing, adaptation, distribution and reproduction in any medium or format, as long as you give appropriate credit to the original author(s) and the source, provide a link to the Creative Commons license, and indicate if changes were made. The images or other third party material in this article are included in the article's Creative Commons license, unless indicated otherwise in a credit line to the material. If material is not included in the article's Creative Commons license and your intended use is not permitted by statutory regulation or exceeds the permitted use, you will need to obtain permission directly from the copyright holder. To view a copy of this license, visit <http://creativecommons.org/licenses/by/4.0/>.

© The Author(s) 2021